ApJ accepted
Preprint typeset using LaTeX style emulateapj v. 6/22/04

THE EFFECT OF TYPE Ibc CONTAMINATION IN COSMOLOGICAL SUPERNOVA SAMPLES

N. L. Homeier
Department of Physics and Astronomy, Johns Hopkins University, 3400 North Charles Street, Baltimore, Maryland, 21218-2686
ApJ accepted

ABSTRACT

We explore the effect of contamination of intermediate redshift Type Ia supernova samples by Type Ibc supernovae. Simulating observed samples of Ia and mixed Ibc/Ia populations at a range of redshifts for an underlying cosmological concordance model ($\Omega_m = 0.27$, $\Omega_\Lambda = 0.73$), we find that even small contamination levels, $2-5\%$ may bias the derived Ω_Λ and Ω_m towards larger values. We thus emphasize the need for clean samples of Type Ia SNe for accurate measurements of the cosmological parameters. We also simulate a SN sample similar to the fiducial SNAP detected distribution (Kim et al. 2004), but include Ibc contamination. For this distribution we illustrate the effect of Ibc contamination on the distance modulus vs. redshift diagram for low and high precision measurements.

Subject headings: cosmological parameters — cosmology: observations — supernovae: general — surveys

1. INTRODUCTION

Type Ia supernovae (SNe) are considered astronomical standard candles and have been used to measure the geometry and dynamics of the Universe (Riess et al. 1998; Perlmutter et al. 1999). This exceedingly difficult measurement relies on observations of local supernovae samples to calibrate relationships between absolute peak magnitude and more easily obtained observables such as light-curve width, color, etc. (see Leibundgut (2001) for a review). These calibrations are then applied to the observables in higher redshift samples to derive distance moduli. Due to the extreme faintness of intermediate to high redshift SN and the shifting of identifying spectral features outside the optical window, spectroscopic classification becomes difficult, and photometry must often suffice. Fortunately, there is a clear observational difference between hydrogen-rich (Type II) and hydrogen-poor (Ia, Ib, and Ic) SNe, namely, the UV deficit (UV radiation is blocked in hydrogen-poor SN explosions by metal lines). This property can be used to distinguish between Type I and II SNe explosions. To date there is no photometric technique to distinguish between Type Ia and Ibc SN (although see Gal-Yam et al., 2004), and one must perform a spectroscopic classification. The characteristic spectroscopic difference between Type Ia and Ibc SNe is the deep absorption trough at 6140Å in Ia spectra, which is due to the blueshifted Si II $\lambda\lambda 6347, 6371$Å feature. Unfortunately this is redshifted out of the optical passband for $z > 0.5$, making classification of Type I SNe difficult. Alternative spectral discriminants between Ia and Ibc SNe are Si II $\lambda 4130$ (e.g. Coil et al. 2000), Fe II $\lambda 4555$ and Mg II $\lambda 4481$ (Barris et al. 2004). Spectroscopic identifications are made using template-matching, but no statistical information is given about misidentifications with this method (Tonry et al. 2003; Riess et al. 2004b; Barris et al. 2004).

Assuming the same relative Ia and Ibc rates in nearby SNe samples, Riess et. al (2004) and Barris et al. (2004) reasoned that the rate of contamination from Type Ibc SN in high redshift samples should be less than $\sim 10\%$. However, the star formation rate increases rapidly at up to $z \sim 1-2$, and this is likely to have a significant effect on the relative rates of SN types. As Type Ibc SNe come from massive stars ($M > 20-30\ M_\odot$), their rate depends on the star formation rate in the previous 10 Myr. It is well established that the global star formation rate increases at higher redshifts. Hence, assuming a delay for Ia explosions, we expect that the rate of Type Ibc SNe increases over the short term, and that the contribution from Ibc SNe becomes more important at higher redshift. Motivated by this, we investigate here what effect contamination by Type Ibc SNe has on cosmological parameters derived from Ia SNe samples. The optimal way to determine the systematic effect in a particular survey is through simulations using the diagnostic machinery associated with said survey. However, the general nature of the effect can be investigated robustly with simulations such as the one we present here.

2. THE GLOBAL STAR FORMATION RATE

The global star formation rate peaked somewhere between $z \sim 1-2$ and has been declining to the present day (Lilly et al. 1996; Madau, Pozzetti, & Dickinson 1998; Steidel et al. 1999; Thompson, Weymann, & Storrie-Lombardi 2001; Bouwens et al. 2003). Between the local Universe and $z \approx 1.5$, the star formation rate increased to $10-20$ times the rate in the current epoch. This significant increase in star formation rate should have a substantial effect on the relative rates of SN types. If the rates are about 1 Type Ibc SN for every 9 of Type Ia, when the star formation rate was 10 times its present value, the rates of Type Ibc and Ia SN should be about equal; for higher star formation rates, Type Ibc SN will outnumber those of Type Ia. Here we assume that the rate of Type Ibc SN explosions does not evolve with metallicity, therefore it depends only on the number of massive stars formed in the last $1-10$ Myr, and thus scales linearly with the recent star formation rate. We also assume that the rate of Type Ia SN should be relatively constant after the "time delay" until the first explosion, which is somewhat speculative. It is possible that the rate of Type Ia SNe correlates with the star formation rate to some degree, but in any case

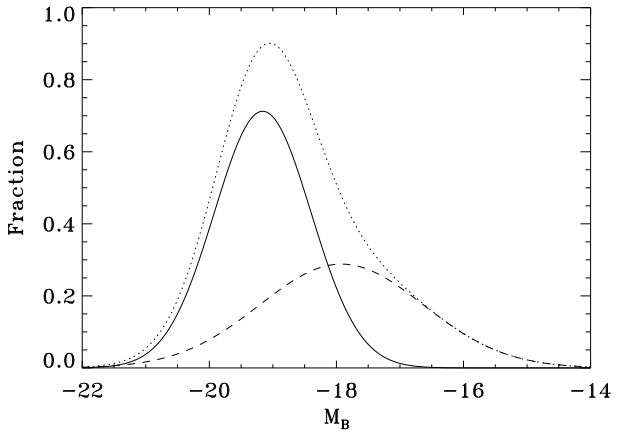

FIG. 1.— Magnitude distribution function for Type Ia and Ibc SNe assuming equal numbers of each and a single gaussian distribution for Type Ibc SNe.

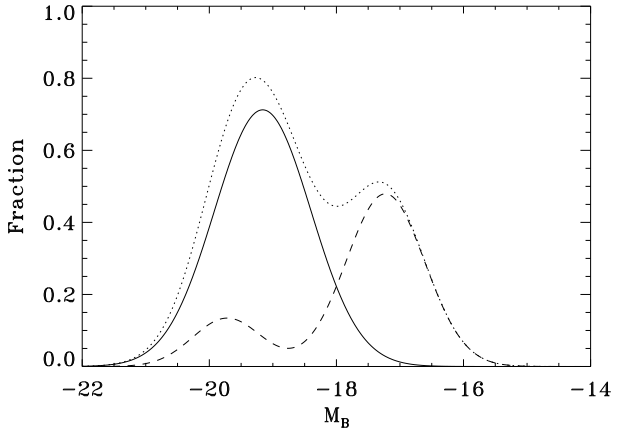

FIG. 2.— Magnitude distribution function for Type Ia and Ibc SN assuming equal numbers of each and a double gaussian distribution with "bright" and "normal" Type Ibc SN.

to a lesser degree than the core-collapse Type Ibc SNe. Whatever the actual degree, an increase in the global star formation rate will affect the relative ratio of Type Ia to Ibc SNe observed at that epoch, which leads us to the present investigation. Important constraints on the time delay for SNe Ia explosion are now being extracted from intermediate redshift SNe samples (Dahlén et al. 2004; Strolger et al. 2004). However, it is important to note that the general conclusions presented here *do not depend* on the Type Ia vs. Ibc rate with star formation rate, only that an increasing Ibc/Ia rate with redshift provided the motivation for this study.

3. ESTIMATING THE EFFECT OF Ibc CONTAMINATION

3.1. *Absolute Magnitude Distributions*

We use the observed distribution of uncorrected absolute magnitudes, from the Richardson et al. (2002) study of the Asiago Supernova Catalog. Pertinent here are the 111 Type Ia SN, 5 luminous Type Ibc SN, and 13 "normal" Type Ibc SN in the catalog. We will use their single gaussian fit to the *uncorrected* absolute magnitudes of the 111 Type Ia SN ($M_B = -19.16, \sigma = 0.76$) and their single gaussian fit to the Type Ibc SNe ($M_B = -18.92, \sigma = 1.29$); these are shown in Figure 1. The number of Type Ibc SNe in the sample is small enough that a two-component model for the distribution of magnitudes is equally valid, with $M_{B1} = -17.23, \sigma_1 = 0.62$; $M_{B2} = -19.72, \sigma_2 = 0.54$, and a weight= 0.28. We run models with both the one and two gaussian distributions for Ibc magnitudes.

3.2. *Method*

We use a Monte Carlo simulation that creates a random redshift array from $z = 0.5 - 3$. Absolute magnitudes are assigned from the Type Ia and Ibc absolute magnitude distributions (described in the preceding section). We then include "observational scatter" by adding or subtracting flux from each object according to a gaussian distribution with $\sigma = 0.35$ magnitudes. This is slightly larger than the mean error of SNe between $z = 0.5 - 2$ in the Tonry et al. (2003) sample (32 objects, mean error= 0.30).

We "observe" objects by calculating the luminosity distance for each object at its individual redshift, and "detecting" those with absolute magnitudes brighter than the detection limit, which we take as $m_B = 25$. This should be roughly correct for redshifts up to $z = 1$. Beyond this, rest-frame B corresponds most closely to J, and $M_J = 24$ is a more realistic limit. However, including this effect does not significantly affect the results in what follows.

The Type Ia SNe that are "detected" are re-sampled to a Gaussian distribution with a center at what we take as the corrected Type Ia SNe absolute magnitude (-19.41; Leibundgut 2001), but with the dispersion equal to quadrature addition of the corrected dispersion of a typical low-redshift SNe sample (0.14; Barris et al. 2004) and an additional observational scatter. This simulates the corrections made to the Type Ia absolute magnitudes based on light curve width and color, but with a larger scatter to simulate observational error. Distance moduli are calculated for each object by assuming each has the absolute magnitude of a corrected Type Ia SN. Then the difference between these distance moduli and the distance moduli for an empty universe is calculated.

High redshift supernovae surveys utilize an analysis method based on the 'Multiwavelength' or 'Multicolor Light-curve Shape Method' (Riess et al. 2004b; Barris et al. 2004). This method uses a set of Ia lightcurves as templates for training, then concurrently fits the distance modulus, extinction, typically expressed in units of A_V, and Δ, a parameter which describes the lightcurve shape and corresponds to the difference in absolute magnitude of the SN and a fiducial SN Ia.

The dominant correction comes from the correlation between light curve shape and peak magnitude, in the sense that fainter Ia SNe decline in luminosity faster than brighter ones. In order to discuss this quantitatively, we consider here the decline parameter, Δm_{15}, which is the difference between the peak magnitude and the magnitude at 15 days after maximum (e.g. Phillips 1993). The decline parameter varies with the observed restframe wavelength, and depends on K-corrections, extinction, and redshift (time dilation) (Nugent, Kim, & Perlmutter 2002). The goal here is not to reproduce a particular

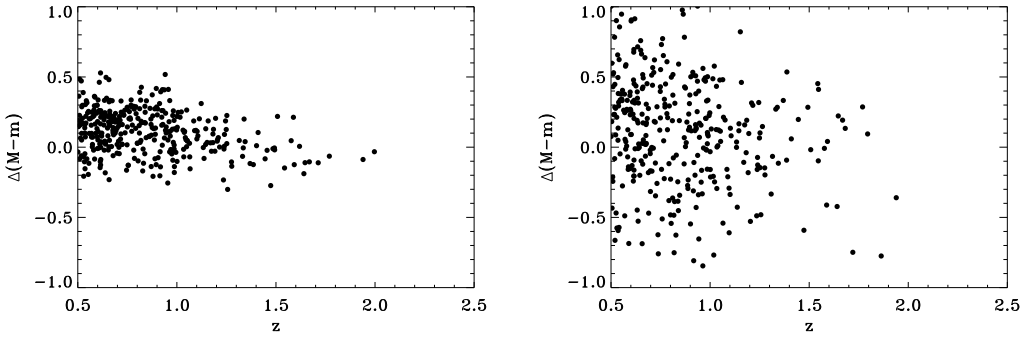

FIG. 3.— An example of detected SN redshift distributions (1000 input, $320-360$ detected) SNe and varying the "observational scatter" from (a) 0.05, where one is dominated by Ia magnitude corrections, $\sigma = 0.14$ and (b) 0.35, where the observational scatter dominates. Input $(\Omega_M, \Omega_\Lambda) = (0.27, 0.73)$.

survey and its associated completeness and bias, but to investigate any possible systematic effect a contaminated SNe sample has on the derived cosmological parameters. Therefore, in this study we assume that the corrections (K, extinction, and time dilation) are accurately performed and the errors associated with these corrections are contained in the observational scatter parameter.

To estimate typical modifications to Ibc magnitudes, we use the relation from Hamuy et al. (1996) for the B-band, $M_{MAX} = a + b[\Delta m_{15}(B) - 1.1]$, where $b = 0.784$, and we set a to the value we use for corrected peak Ia magnitudes, -19.41. We stress that the particular values for M_{MAX}, dispersions, etc. that we use are not significant, only that we consistently use the same values throughout the simulation. Then we need typical decline parameters for Ibc SNe. Most published lightcurves for Ib and Ic SNe are not well-sampled in the period ± 30 days from maximum, but focus on the long-term behavior of the lightcurve. We have collected a sample of 5 Ibc lightcurves with measurable Δm_{15}; these are summarized in Table 3.3. We also note that we have not listed the Ib SN 1983N (Clocchiatti et al. 1996) and Ic SN 1983V (Clocchiatti et al. 1997) that have been shown to have similar lightcurves to SN 1993J, although the number of photometric points in the first ± 30 days is small.

SN	Type	ΔM_{15}	$M_{B,max}$	$B_{max} - V_{max}$	Ref
1990B	Ic	0.964 (B)	–	–	(1), (2)
		1.14 (R)			
1992ar	Ic		-19.7 ± 0.5	0.4 ± 0.2	(3)
1994I	Ic	2.07 ± 0.03 (B)	-17.68 ± 0.73	0.15*	(4)
1993J	IIb	2.5 (B)	-17.3 ± 0.6	0.18*	(6)
		0.95 (V)			(6)
		0.8 (R)			(6)
1998dt	Ib	0.2-0.3 (R)	–	–	(2)
1999di	Ib	0.4 (R)	–	–	(2)
1999dn	Ib	0.5 (R)	–	–	(2)
1999ex	Ic		−17.4	0.42	(7)
1999bw	Ic	1.0 (B)	−18.88	0.4	(8)

*Corrected for extinction, (1) Clocchiatti et al. (2001), (2) Matheson et al. (2001), (3) Clocchiatti et al. (2000), (4) Clocchiatti et al. (1996) (5) Richmond et al. (1996), (6) Richmond et al. (1994), (7) Stritzinger et al. (2002) (8) Galama et al. (1998)

3.3. *Decline Parameters*

Decline parameters for these 5 Ibc SNe span a wide range of values. In light of this, we select reasonable ranges for the decline parameter considering the sample of Ia SNe presented in Hamuy et al. (1996). We emphasize that this is valid even if decline parameters for Ibc SNe are distributed differently than Ia decline parameters, as Ibc SNe that are not weeded out will be fit to Ia templates. We explore four treatments assuming: (1) no modifications, (2) all Ibc SNe are matched to templates with small decline parameters (mean=0.9, dispersion=0.1), (3) all Ibc SNe are matched to templates with large decline parameters (mean=1.5, dispersion=0.3), and (4) Ibc SNe are matched with decline parameters with a mean of 1.1 and a gaussian dispersion of 0.3. This leads to mean assumed absolute magnitudes of (1) −19.41 (2) −19.57, (3) −19.10, and (4) −19.41 (same as (1)).

We compare these simulated data to a grid of models with a range of Ω_m and Ω_λ values, and calculate the corresponding grid of χ^2 values. Probability curves are calculated from this χ^2 grid following the method of Tonry et al. (2003). That is, the minimum in the χ^2 array is found, and a grid of probabilities is calculated where prob=exp$(-0.5 \times (\chi^2 - min(\chi^2))$. The levels of 68%, 95%, and 99.5% are found by integrating (summing) the probability array and identifying where 68%, 95%, and 99.5% of the total probability are located. This is only valid when the minimum reduced χ^2 is close to 1 (as it is in the SNe sample analyzed in Tonry et al. (2003)).

4. RESULTS

4.1. *Malmquist Bias with Ibc SNe*

In Figure 4 we show the change in the measured mean distance modulus (compared to an empty universe or eternally coasting model) from our simulation for *input* Ibc/Ia ratios of 0.1, 0.5, and 1.0 and an underlying concordance model with $(\Omega_m, \Omega_\Lambda) = (0.27, 0.73)$. An interesting effect can be seen, which is solely due to the observational apparent magnitude limit. At redshifts less than ~ 0.8, the mean distance modulus is fainter than the pure Ia case, and at redshifts greater than this it is brighter.

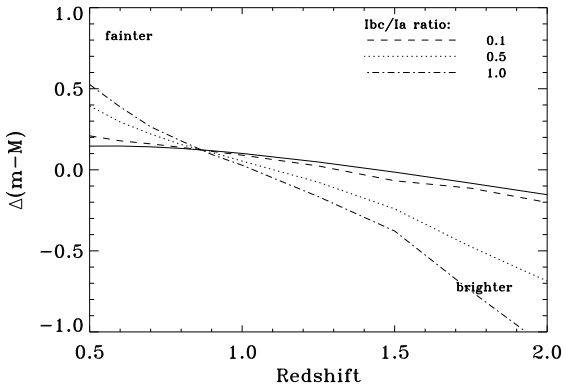

FIG. 4.— Change in the mean measured distance modulus for Ibc/Ia ratios of 0.1, 0.5, and 1.0. This is shown only for purposes of illustration.

This is because of the luminosity distribution of Type Ibc SNe, with the majority being fainter than Type Ia SNe. At lower redshifts, Ibc contamination pushes the mean fainter, while at higher redshifts, these fainter SNe are below the detection limit, and only the brightest SNe are detected, pushing the mean to apparently brighter magnitudes. The transition point is set by the apparent magnitude limit, here taken as $m_B = 25.$, and moves to higher redshift at fainter apparent magnitude limits, and vice versa. This is shown only for illustrative purposes, and no conclusions are derived from this diagram.

4.2. *Stochasticity*

The number of detected SNe affects the spacing of the probability curves, but more importantly, it affects the variation in the location of the χ^2 minimum from run to run. As expected, with smaller numbers of detected SNe, the curves are unstable, and "jump around" from run to run. As the number of input SNe is increased, and thus the number of detected SNe also increases, the position of the curves is more stable.

As an example of this, for 100 trials using 500 Type Ia SNe uniformly and randomly distributed between z= $0.5 - 2.0$, with a mean of 190.04 detected SNe, the mean Ω_m, Ω_Λ values at the location of the χ^2 minima were 0.269 and 0.733, with standard deviations of 0.103 and 0.181. The mean minimum reduced χ^2 was 1.01, with a standard deviation of 0.11. Inputing 5000 Type Ia SNe in 100 trials with a mean of 1884.07 detected SNe decreased the standard deviations to 0.034 and 0.064, with mean Ω_m, Ω_Λ values of 0.27 and 0.73. The mean minimum χ^2/N was 1.007, with a standard deviation of 0.031.

We investigated what effect Type Ibc SNe would have on the derived probability curves by assuming values of 0.27 and 0.73 for Ω_m and Ω_Λ (the 'cosmological concordance' model) and distributing 2000 Type Ia SNe uniformly and randomly between $z = 0.5 - 2$. In one run of the simulation, 724 of the 2000 were "detected", and the probability curves corresponding to the χ^2 analysis are shown in Figure 5(a). Using these same 2000/724 Type Ia SNe, we first added 100 Type Ibc SNe with magnitudes distributed randomly according to the unimodal distribution presented in § 3.1. 11 of these were "detected", and the result of this simulation is shown in Figure 5(b). In Figure 5(c) we show the result of using 200 Type Ibc SNe (input ratio of 10%), of which 26 were detected. The reduced χ^2 increased from 0.97 for the pure Ia sample, to 1.13 for the sample used in Figure 5(b), to 1.36 at a contamination level of only 5%, shown in Figure 5(c).

In these simulations, relatively low contamination rates of 26/742=4% significantly affect the location of the probability curves in the Ω_M, Ω_Λ plane, moving both Ω_M, Ω_Λ to higher values. However, as the fraction of detected Type Ibc SNe increases, the minimum reduced χ^2 value also increases. At some point, this minimum reduced χ^2 value should be large enough that one would correctly conclude that the model is not a good fit, and the conversion from the χ^2 grid to probability curves would not be, and should not be, attempted without first renormalizing the errors. Then the probability contours become larger, and should encompass the correct Ω_M, Ω_Λ values. However, in this renormalization it is implicit that the model is a good fit, and the random errors are underestimated. In this example, this is incorrect.

The spacing of the probability curves changes with the value of the observational scatter and the total number of SNe detected. But the stability of the location of the center of the curves depends on the number of detected SNe, varying stochastically. We find that for large samples with relatively accurate measurements, even a small contamination ($2-3\%$) of Type Ibc SNe can significantly bias the result. In 100 trials with an input of 5000 SNe uniformly and randomly distributed between z= $0.5-2.0$, an observational scatter of 0.35, an input Ibc/Ia ratio of 0.1, and a bimodal magnitude distribution (resulting in a mean of 1891.05 Type Ia and 54.61 Type Ibc SNe detected), the mean Ω_m, Ω_Λ values for the location of the χ^2 minimum were 0.334 and 0.826, with standard deviations of 0.038 and 0.069. The minimum reduced χ^2 was 1.156, with a standard deviation of 0.048. In this case, the underlying values of $\Omega_m = 0.23, \Omega_\Lambda = 0.73$ are outside the 1σ curves, but inside the 2σ curves, 68% of the time.

It is worth noting that the minimum χ^2 is at $(\Omega_m, \Omega_\Lambda) \sim (1.3, 0.6)$ for the Tonry et al. (2003) sample, before applying external constraints. In fact, without external constraints, the "concordance model" values are outside the 1σ contours. However, in Riess et al. (2004b) and Barris et al. (2004), the error contours are significantly larger, and encompass the concordance model values for the density parameters.

4.3. *Unimodality vs. Bimodality*

We also compared the effects of single and double gaussian Ibc magnitude distributions. These results are summarized in Table 1. With a single gaussian distribution, stochastic effects are more important, as illustrated by the larger standard deviations for the mean recovered Ω_M, Ω_Λ, and minimum χ^2/N. In terms of systematic error in the recovered cosmological parameters, if the double gaussian distribution for Ibc magnitudes is more accurate in describing the underlying distribution, contamination by Ibc SNe will bias the results less severely than the single gaussian case.

4.4. *Effect of Decline Parameters*

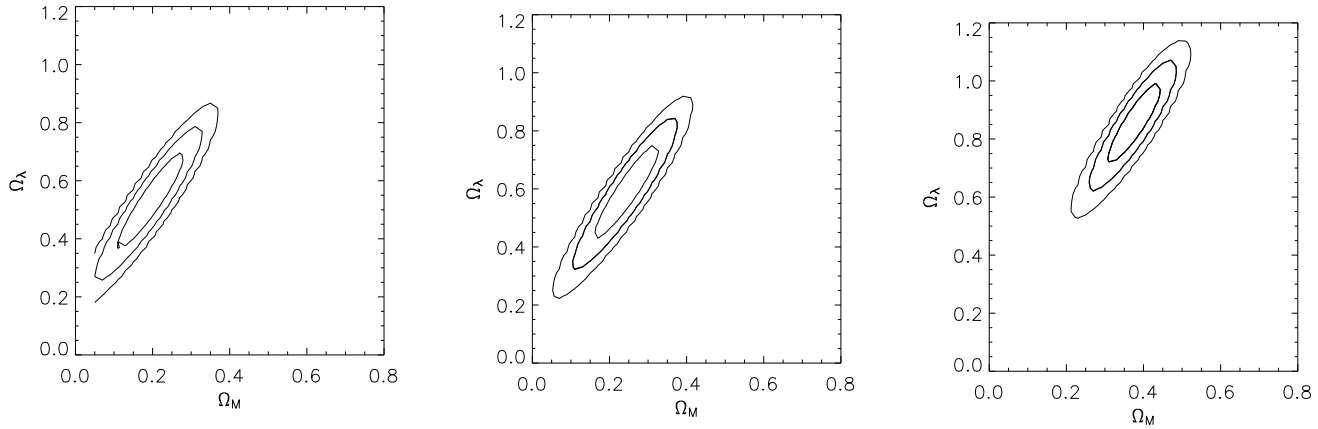

FIG. 5.— Input of 2000 Ia uniformly and randomly distributed from z= $0.5-2$ and a single gaussian distribution of (b) 100 Ibc and (c) 200 Ibc. (a) 724 detected Type Ia SNe. The minimum reduced χ^2 is 1.03. (b) 724 detected Type Ia SNe, 11 Ibc SNe. The minimum reduced χ^2 is 1.13. (c) 724 detected Type Ia SNe, 26 detected Ibc SNe. The minimum reduced χ^2 is 1.36.

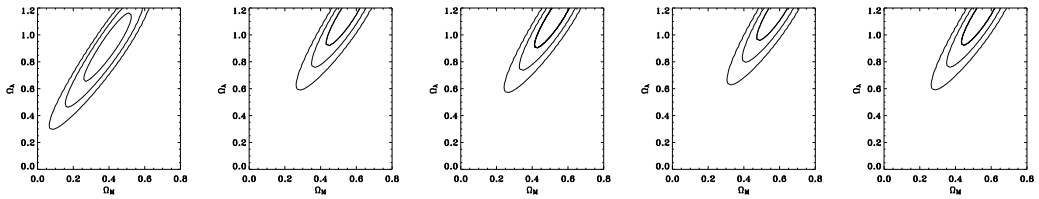

FIG. 6.— See text for details. From left to right: (a) 231 Ia SNe, (b) 231 Ia, 15 Ibc with no modification to the Ibc magnitudes, (c) 231 Ia, 15 Ibc with modification with small decline parameters, (d) 231 Ia, 15 Ibc with modification with large decline parameters, (e) 231 Ia, 15 Ibc with modification with medium decline parameters. There is no significant difference between scenarios with this range of Ibc magnitude modifications.

TABLE 1
A COMPARISON OF THE MAGNITUDE DISTRIBUTIONS FOR IBC SUPERNOVAE. RESULTS FROM 100 TRIALS.

	single gaussian	double gaussian
mean Ω_M	0.409 ± 0.126	0.344 ± 0.094
mean Ω_Λ	0.974 ± 0.243	0.839 ± 0.176
mean minimum χ^2/N	1.393 ± 0.242	1.225 ± 0.110
mean number of SNe Ia detected	228.77	226.78
mean number of SNe Ibc detected	12.46	10.26

We explore four treatments assuming: (1) no modifications to Ibc magnitudes, (2) all Ibc SNe are matched to templates with small decline parameters (mean=0.9, dispersion=0.1), (3) all Ibc SNe are matched to templates with large decline parameters (mean=1.5, dispersion=0.3), and (4) Ibc SNe are matched with decline parameters with a mean of 1.1 and a gaussian dispersion of 0.3. This leads to mean assumed absolute magnitudes of (1) −19.41 (2) −19.57, (3) −19.10, and (4) −19.41 (same as (1)).

In Figure 6 we compare the results for a single case for these four treatments. The number of detected SNe was 231 Ia and 15 Ibc. Assuming Ibc SNe are treated as Ia SNe or the magnitudes are not modified does not have a significant effect. The corrections to the magnitudes are negligible compared to the magnitude difference between the detected Ia and Ibc SNe.

4.5. *Colors*

From the sample of SNe compiled in Table 3.3, we find that the $B_{max} - V_{max}$ colors of Ibc SNe have a tendency to have redder colors than Ia SNe, which typically have $B_{max} - V_{max} \sim 1$. However, the slope of the relation of $B - V$ color with time from maximum is similar, as illustrated in Figure 15 of Stritzinger et al. (2002) for SN1999ee (Ia) and SN1999ex (Ib/c). If the maximum was not observed, a shift of ~ 15 days would place the two $B - V$ curves on top of one another.

If the $B_{max} - V_{max}$ color is correctly measured through an accurate determination of the date at maximum, then an interloping Ibc SN will appear redder than the average Ia SN. If this Ibc SN has a large decline parameter, it will be "expected" to be fainter, and fainter Ia SNe are redder at maximum (see Figure 1 of Riess, Press, & Kirshner (1996) for examples). However, if this Ibc SN has a small decline parameter, it will be "expected" to be brighter, and brighter SNe are bluer. Therefore, the red color will be interpreted as due to extinction.

As an example, let us consider SN 1998bw (Galama et al. 1998), the first confirmed supernova/GRB. This supernova had a decline parameter $\Delta m_{15} = 1.0$, $B_{max} - V_{max}$ of 0.4 magnitudes, and $M_{B_{max}} = -18.88$. If the intrinsic color was assumed to

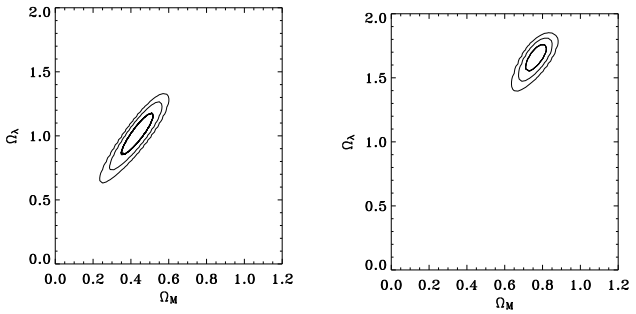

FIG. 7.— Including a changing star formation rate with redshift with a single gaussian Ibc magnitude distribution. In (a), the rate of Type Ibc to Ia SNe follows the dependence $0.05(1+z)$, while in (b) it varies as $0.1(1+z)$, the same redshift dependence but with a different normalization. The number of detected Ia and Ibc SNe was (a) Ia= 318, Ibc= 20, and (b) Ia= 287, Ibc= 41. The minimum χ^2/N is (a) 1.57 and (b) 2.27.

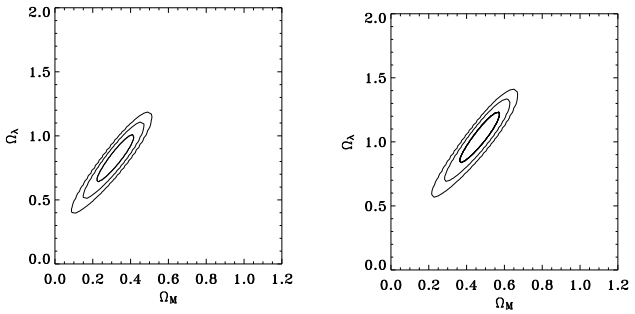

FIG. 8.— Including a changing star formation rate with redshift with a two gaussian Ibc magnitude distribution. The Ia distribution is identical to that in Figure 7. In (a), the rate of Type Ibc to Ia SNe follows the dependence $0.05(1+z)$, while in (b) it varies as $0.1(1+z)$, the same redshift dependence but with a different normalization. The number of detected Ia and Ibc SNe was (a) Ia= 318, Ibc= 15, and (b) Ia= 287, Ibc= 32. The minimum χ^2/N is (a) 1.21 and (b) 1.52.

be $B_{max} - V_{max} = 0$, then $E(B-V) = 0.4$, $A_V = 1.24$, and $A_B = 1.64$. The observed apparent rest-frame B magnitude would be corrected by approximately 1.6 magnitudes, and the derived distance modulus would be too large by more than 1 magnitude. Put another way, this object would appear 1 magnitude brighter than an accurately corrected Ia SN.

This effect should act in a random way, unless the peak magnitudes, colors, and light curve shapes of Ibc SNe are correlated. With the current available sample in the literature, we are unable to determine the relationship between these parameters. However, we note that some type Ia SNe have $B_{max} - V_{max}$ colors similar to those of Ibc SNe, for example, 1990Y, 1992K, and 1993H (Hamuy et al. 1996). If these or similar lightcurves are used as templates in the fitting procedure, then the argument in the previous paragraphs is negated. For our example Ic SN 1998bw, the "corrected" mag would be approximately 0.6 magnitudes too faint. In this case, the effect of intrinsic $B_{max} - V_{max}$ colors, which do appear to be different for Ia and Ibc SNe, can only be correctly assessed by testing the template fitting codes of individual surveys. We urge investigators to consider testing the robustness of their photometric and spectroscopic fitting to Ibc interlopers.

4.6. *SFR(z), Ibc/Ia(z)*

We also investigated a Ibc/Ia ratio that changes with redshift. In Figure 7 we present examples of including a dependence of the Ibc/Ia ratio with redshift, mimicking a dependence on the star formation rate. Due to the severe effect of Ibc contamination on the probability curves even for small levels of contamination, we were forced to keep the relationship shallow $(1+z)$ and with a small Ibc/Ia normalization ratio (≤ 0.1). In Figure 7, the minimum reduced χ^2 was 1.5. However, for the case shown in Figure 8, the minimum reduced χ^2 was 2.6, and the simple calculation of probability curves we have shown is not valid. A more sophisticated treatment using the estimated Ia and non-Ia SNe rates with redshift from Dahlén et al. (2004) could be performed, but the measurements are so sensitive to Ibc contamination that a more complex treatment is unwarranted.

4.7. *Comparison to the SNAP Redshift Distribution*

Kim et al. (2004) reviewed systematic uncertainties in SNe studies to determine the cosmological parameters. In their study, a fiducial number-redshift distribution for SNe was used, an observational scatter of 0.1 magnitudes, and a dispersion about the corrected Ia peak magnitudes of 0.1 magnitudes. We would like to use the same SNe-redshift distribution to see what effect Ibc contamination would have. However, including the redshift distribution of detected SNe is problematic, as instead of specifying detected SNe, we assign an input distribution, then "observe" those above our apparent magnitude limit. To accurately determine the effects of Ibc contamination, an apparent magnitude limit must be included, thus some "observation" must be simulated. To match the $SNAP$ fiducial distribution, we tailor the input distribution such that the "observed" distribution is sufficiently similar to the fiducial $SNAP$ distribution.

We attempt to reproduce the $SNAP$ fiducial distribution's general increase in numbers from $z = 0.1-0.8$, the peak near z=0.8, and the slope of the decline in numbers from $z = 0.8-1.7$, $dlogN(z)/dz = -0.4$. The solution of input to detected numbers is not general, but depends on the detection limit. For $m_B = 25.$, we find a reasonable agreement with an input of two power law distributions, 700 SNe between $z = 0.1-1.0$ as $N \propto z^2$, and 10000 between $z = 0.8-1.7$ as $N \propto z^5$. We then input 1000 Ibc SNe between $z = 0.8-1.7$ as $N \propto z^5$, the same relationship as for the high redshift Ia population. Thus, we include an underlying ratio of 0.1 for Ibc/Ia SNe. An example of a final detected redshift distribution is shown in Figure 9(a), and the $\Delta(m-M)$ vs. z distribution in Figure 9(b). We emphasize that this is one run of a Monte Carlo code, and as in every random process, each individual answer is different.

An important issue is clearly illustrated in Figure 9; if the observational scatter and the dispersion about the corrected peak magnitudes is low, 0.1 magnitudes for each in this simulation, then Ibc SNe are easily distinguished. Even when the number of SNe is low, the bright Ibc SNe that bias measurements of the cosmological parameters are easily isolated. On the other hand, when

the observational scatter is large, large numbers of SNe are needed to identify outliers, in this case Ibc SNe. This is illustrated in Figure 10.

If such a low scatter and corrected dispersion is feasible, then the need for spectra of SNe candidates to determine Ia-ness is eliminated. Depending on the distribution of SNe, such a survey could possibly rely instead on rejecting 3σ outliers from the mean or median distance modulus in a given redshift bin. Even if the observational scatter is ~ 0.3, if the numbers are large, then σ-clipping is still a valid option to remove outliers, however, the constraints on the cosmological parameters will not improve, as the probability curves will not shrink. The important question becomes, is such precision feasible? The answer to this question is best left to survey designers.

5. ON THE LIKELIHOOD OF Ibc CONTAMINATION

As the progenitors of Type Ibc SNe are massive stars, we can expect that the majority have higher extinctions than Ia SNe and occur in gas-rich galaxies. Thus, excluding SNe with high derived A_V values and those occuring in late-type host galaxies should reject more Ibc SNe than Ia and reduce contamination. However, the SN rate in different galaxy types as a function of redshift is not known. Although the local Ibc/Ia rate is ~ 0.1, we can expect this to increase to $0.5 - 1.0$ around $z = 1$. Assuming no evolution in the luminosity functions, this means $1 - 3$ *bright* Ibc SNe for every 10 Ia. For Ibc contamination to be a significant concern, $20 - 50\%$ of these *bright* Ibc SNe must fail to be rejected through the possible combinations of light curve fitting, spectral-typing, host galaxy morphology, and extinction. The likelihood of this could be determined through detailed simulations using Ibc templates (e.g. 1999bw, 1992ar) and routines such as MLCS2k2 (Riess et al. 2004b), or BATM (Tonry et al. 2003).

6. CONCLUSIONS

We find that even small contamination fractions (5%) may bias the measurement of Ω_M and Ω_Λ. However, we have also illustrated the ease with which Ibc SNe can be identified when the observational error and the dispersion about the corrected Ia peak magnitudes is low. Based on the calculations presented here, the straightforward effect of contamination from Type Ibc SN in intermediate-to-high redshift SN samples is to reduce the χ^2 goodness-of-fit to the true cosmological parameters. This manifests itself as an increase in the minimum value of the reduced χ^2 grid. For a flat universe with $\Omega_M = 0.27, \Omega_\Lambda = 0.73$ even small numbers (5%) of Type Ibc SNe may push both values upwards. Erroneously small "probability" curves can be generated by assuming the model is a good fit and that the minimum reduced χ^2 is close enough to 1 for a meaningful conversion to a probability grid. However, if the observational errors are large, it is difficult to distinguish between a minimum reduced χ^2 that is larger due to a mismatch of the model and the observations due to contamination or from simple stochastic effects.

If the observational errors are large enough (> 0.3), then a small contamination fraction (5%) by Ibc SNe can shift the location of the χ^2 minimum without making χ^2 itself large. In such a case the error contours will be large, so while the contours are not strictly statistically correct, they are still meaningful in the sense that the underlying cosmological parameters have close to a 99% chance of being within the 2σ contours. If the observational error approaches the scatter in the corrected 'standard candle' Ia magnitudes, the errors bars will shrink. However, with the same amount of Ibc contamination, as the observational error steadily decreases, the reduced χ^2 becomes steadily greater than 1. Then the conversion from a χ^2 grid to probabilities is not valid. One may assume that the random errors are underestimated and renormalize; the error contours may then become large enough to encompass the underlying Ω_M, Ω_Λ values. But if this precision is achieved, outliers should already be readily discriminated in the $\Delta(m - M)$ vs. z plane, and a simple $3 - 5\sigma$ clipping routine may suffice. Simply having large numbers of SNe with the precision of current surveys would also allow one to use σ-clipping to remove Ibc outliers, however, this will not achieve significantly greater precision in the measurement of cosmological parameters.

The author is pleased to acknowledge the anonymous referee for comments and suggestions which improved the content of the paper. Thank you to T. Matheson for providing lightcurve data and reference pointers for Ib/c SNe, and A. Riess for useful comments on how SN typing is performed. The author would also like to thank B. Leibundgut for comments on an early version of this manuscript, J. Tonry for providing his code for perusal, and especially hearty thank-yous to T. Puzia, J. Blakeslee, and M. Livio for critical readings and comments. This work was supported in part by generous scientific freedom granted by H. Ford, for which the author is grateful.

REFERENCES

Barris, B. J., et al. 2004, ApJ, 602, 571
Blakeslee, J. P. et al. 2003, ApJ, 589, 693
Bouwens, R. J. et al. 2003, ApJ, 595, 589
Clocchiatti, A., et al. 1996, AJ, 111, 1286
Clocchiatti, A., et al. 1997, ApJ, 483, 675
Clocchiatti, A., et al. 2000, ApJ, 529, 661
Clocchiatti, A., et al. 2001, ApJ, 553, 886
Coil, A. L., et al. 2000, ApJ, 544, L111
Dahlén, T., et al. 2004, ApJ, in press
Galama, T. J., et al. 1998, Nature, 395, 670
Gal-Yam, A., Poznanski, D., Maoz, D., Filippenko, A. V., & Foley, R. J 2004, PASP, in press
Hamuy, M., Phillips, M. M., Suntzeff, N. B., Schommer, R. A., Maza, J., & Aviles, R. 1996, AJ, 112, 2391
Kim, A. G., Linder, E. V., Miquel, R., & Mostek, N. 2004, MNRAS, 347, 909
Leibundgut, B. 2001, ARA&A, 39, 67
Lilly, S. J., Le Fevre, O., Hammer, F., & Crampton, D. 1996, ApJ, 460, L1
Madau, P., Pozzetti, L., & Dickinson, M. 1998, ApJ, 498, 106
Matheson, T., Filippenko, A. V., Li, W., Leonard, D. C., & Shields, J. C. 2001, AJ, 121, 1648
Nugent, P., Kim, A., & Perlmutter, S. 2002, PASP, 114, 803
Perlmutter, S. et al. 1999, ApJ, 517, 565
Phillips, M. M. 1993, ApJ, 413, L105
Richardson, D., Branch, D., Casebeer, D., Millard, J., Thomas, R. C., & Baron, E. 2002, AJ, 123, 745

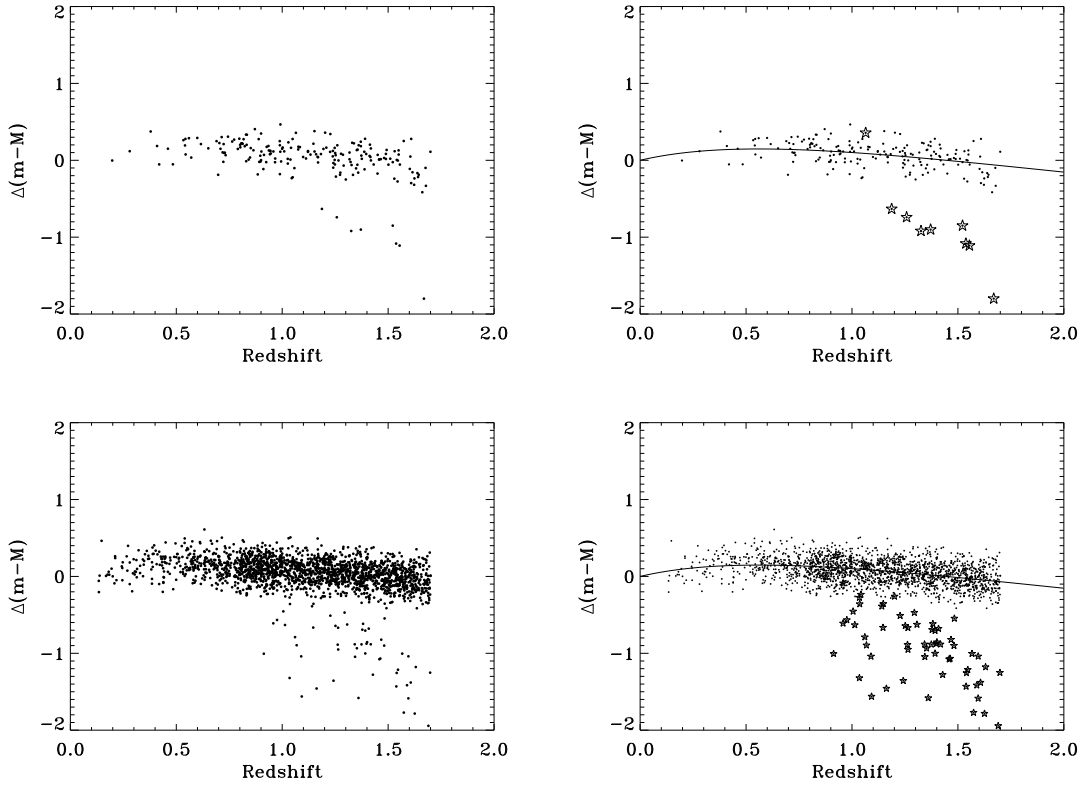

FIG. 9.— Observational scatter of 0.1 magnitudes. Top panels: 188 detected Ia, 9 Ibc, bottom panels: 1922 detected Ia, 64 Ibc. Stars in the right panels indicate Ibc SNe.

Richmond, M. W., Treffers, R. R., Filippenko, A. V., Paik, Y., Leibundgut, B., Schulman, E., & Cox, C. V. 1994, AJ, 107, 1022
Richmond, M. W., et al. 1996, AJ, 111, 327
Richmond, M. W., Filippenko, A. V., & Galisky, J. 1998, PASP, 110, 553
Riess, A. G., Press, W. H., & Kirshner, R. P. 1996, ApJ, 473, 88
Riess, A. G. et al. 1998, AJ, 116, 1009
Riess, A. G. et al. 2004a, ApJ, 600, L163
Riess, A. G., et al. 2004b, ApJ, 607, 665
Steidel, C. C., Adelberger, K. L., Giavalisco, M., Dickinson, M., & Pettini, M. 1999, ApJ, 519, 1
Stritzinger, M., et al. 2002, AJ, 124, 2100
Strolger, L .G., et al. 2004, ApJ, in press
Thompson, R. I., Weymann, R. J., & Storrie-Lombardi, L. J. 2001, ApJ, 546, 694
Tonry, J. L. et al. 2003, ApJ, 594, 1

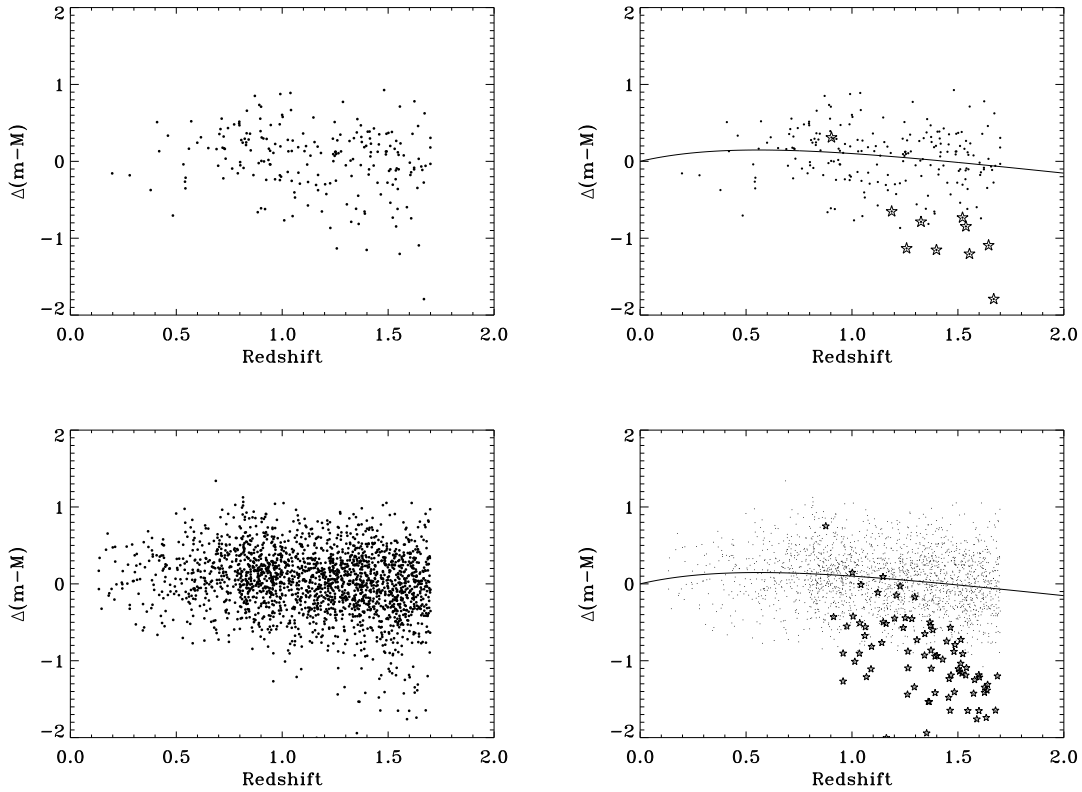

FIG. 10.— Observational scatter of 0.35 magnitudes. top panels: 207 detected Ia, 10 Ibc, bottom panels: 2029 detected Ia, 80 Ibc. Stars in the right panels indicate Ibc SNe.